Ann. Geophys. Discuss., https://doi.org/10.5194/angeo-2018-93
Manuscript under review for journal Ann. Geophys.
Discussion started: 10 September 2018

Annales Geophysicae Discussions

Sensitivity of GNSS tropospheric gradients to processing options

Michal Kačmařík[1], Jan Douša[2], Florian Zus[3], Pavel Václavovic[2], Kyriakos Balidakis[3], Galina Dick[3], Jens Wickert[3,4]

[1] Department of Geoinformatics, VŠB – Technical University of Ostrava, Ostrava, The Czech Republic
[2] Geodetic Observatory Pecný, Research Institute of Geodesy, Topography and Cartography, Zdiby, The Czech Republic
[3] GFZ German Research Centre for Geosciences, Potsdam, Germany
[4] Institute of Geodesy and Geoinformation Science, Technical University of Berlin, Germany

Correspondence to: M. Kačmařík (michal.kacmarik@vsb.cz)

Abstract. An analysis of processing settings impact on estimated tropospheric gradients is presented. The study is based on the benchmark data set collected within the COST GNSS4SWEC action with observations from 430 GNSS reference stations in central Europe for May and June 2013. Tropospheric gradients were estimated in eight different variants of GNSS data processing using Precise Point Positioning with the G-Nut/Tefnut software. The impact of the gradient mapping function, elevation cut-off angle, GNSS constellation and real-time versus post-processing mode were assessed by comparing the variants by each to other and by evaluating them with respect to tropospheric gradients derived from two numerical weather prediction models. Generally, all the solutions in the post-processing mode provided a robust tropospheric gradient estimation with a clear relation to real weather conditions. The quality of tropospheric gradient estimates in real-time mode mainly depends on the actual quality of the real-time orbits and clocks. Best results were achieved using the 3° elevation angle cut-off and a combined GPS+GLONASS constellation. Systematic effects of up to 0.3 mm were observed in estimated tropospheric gradients when using different gradient mapping functions which depend on the applied observation elevation-dependent weighting. While the latitudinal troposphere tilting causes a systematic difference in the north gradient component on a global scale, large local wet gradients pointing to a direction of increased humidity cause systematic differences in both gradient components depending on the gradient direction.

1 Introduction

When processing data from Global Navigation Satellite Systems (GNSS), a total signal delay due to the troposphere is modelled by epoch- and station-wise Zenith Total Delay (ZTD) parameters, and, optimally, together with tropospheric gradients representing the first order asymmetry of the total delay. ZTDs, which are closely related to Integrated Water Vapor (IWV), are operationally assimilated into numerical weather prediction models (NWM) and have been proven to improve precipitation forecasts (Vedel and Huang, 2004, Guerova et al., 2006, Shoji et al., 2009). Previous studies demonstrated that the estimation of tropospheric gradients improves GNSS data processing mainly in terms of receiver position and ZTDs (Chen and Herring, 1997, Bar-Sever et al., 1998, Rothacher and Beutler, 1998, Iwabuchi et al., 2003, Meindl et al., 2004).

Ann. Geophys. Discuss., https://doi.org/10.5194/angeo-2018-93
Manuscript under review for journal Ann. Geophys.
Discussion started: 10 September 2018

Tropospheric gradients are not assimilated into NWMs, however, they are essential for the reconstruction of slant total delays (STD). The STDs represent the signal travel time delay between the satellite and the station due to neutral atmosphere and they are considered useful in numerical weather prediction (Järvinen et al., 2007, Kawabata et al., 2013, Bender et al., 2016) and reconstruction of 3D water vapor fields using the GNSS tomography method (Flores et al., 2000, Bender et al., 2011). Brenot et al. (2013) showed a significant improvement of IWV interpolated 2D fields when tropospheric gradients are taken into account. With the improved IWV fields, the authors studied small scale tropospheric features related to thunderstorms. Douša et al. (2018a) demonstrated the advantage of similar pseudo-observations in the 2-stage troposphere model combining optimally NWM and GNSS data. Morel et al. (2015) presented a comparison study on zenith delays and tropospheric gradients from 13 stations at Corsica Island in the year 2011. Despite a good agreement in the ZTD, they found notable discrepancies in tropospheric gradients estimated using two different GNSS processing software. Besides different processing methods (double-differenced network solution versus Precise Point Positioning, PPP (Zumberge et al., 1997) solution), the two software used different gradient mapping functions. Douša et al. (2017) indicated a problem with systematic errors in tropospheric gradients due to absorbing instrumentation errors. Minimum attempts were made to compare the tropospheric gradients with independent estimates, i.e., those derived from Water Vapor Radiometer (WVR) or NWM data. For a selected number of stations such a comparison was made in Li et al. (2015) to show that with the upcoming finalization of new systems such as Galileo and BeiDou the improved observation geometry yields more robust tropospheric gradient estimates. Another multi-GNSS study on tropospheric gradients (Zhou et al., 2017) used data from a global network of 134 GNSS stations processed in six different constellation combinations in July 2016. An impact of gradients estimation interval (from 1 to 24 h) and cut-off elevation angle (between 3° and 20°) on a repeatability of receiver coordinates was examined. Better results were found for solutions where a shorter time interval of tropospheric gradient estimation was used and where the elevation cut-off angle of 7° was applied. However, systematic errors and impacts of a gradient mapping function or observation weighting have not been studied yet.

In this work, we systematically evaluate the quality of tropospheric gradients estimated from a regional GNSS dense network under different atmospheric conditions. Using a unique data set, we study the impact of several approaches. ZTDs and tropospheric gradients are then compared with the ones estimated from two NWMs – ERA5, which is a global atmospheric reanalysis, and a limited area short range forecast utilizing the Weather Research and Forecasting (WRF) model. Finally, we quantified systematic differences in tropospheric gradients coming from the gradient mapping function and the method of observation weighting during a local event with strong wet gradients.

2 Data and Methods

2.1 Benchmark data set

The benchmark campaign was realized within the European COST Action ES1206 GNSS4SWEC to support development and validation of a variety of GNSS tropospheric products. An area in central Europe covering Germany, the Czech Republic and

Ann. Geophys. Discuss., https://doi.org/10.5194/angeo-2018-93
Manuscript under review for journal Ann. Geophys.
Discussion started: 10 September 2018

part of Poland and Austria was selected as a domain while May and June 2013 as a suitable time period due to occurrence of severe weather events including extensive floods. Data from 430 GNSS stations were collected together with meteorological observations from various instruments (synoptic, radiosonde, WVR, meteorological radar, etc.). In addition, tropospheric parameters from two global and one regional NWMs were generated. Detailed information about the benchmark campaign can be found in Douša et al. (2016). Although the presented study is based on the GNSS data collected within the benchmark campaign, all the presented GNSS and NWM solutions were newly prepared for this study.

2.2 Estimation of tropospheric gradients from GNSS

The STD as a function of the azimuth (a) and elevation (e) angle can be written as follows:

$$STD(a,e) = mfh(e) * ZHD + mfw(e) * ZWD + mfg(e) * (Gn * cos(a) + Ge * sin(a)) + R \quad (1)$$

where ZHD denotes the Zenith Hydrostatic Delay and ZWD denotes the Zenith Wet Delay. The elevation angle dependency is given by mapping functions, which are different for the hydrostatic (*mfh*), wet (*mfw*) and gradient (*mfg*) part. The tropospheric horizontal gradient vector is defined in the local horizontal plane with two components, one for the north-south direction (*Gn*) and one for the east-west direction (*Ge*). The post-fit residual R represents any un-modelled effects (Shoji et al., 2004).

During GNSS data processing, the ZHD is commonly taken from an a priori model, e.g. Saastamoinen (1972) or Global Pressure and Temperature (GPT, Boehm et al., 2007) based on climatological data, or it can be derived from NWM data. The ZWD, or a correction to the modelled ZHD, and tropospheric gradients are estimated as unknown parameters using a deterministic or stochastic model.

Current mapping functions for hydrostatic (*mfh*) and wet (*mfw*) delay components are based either on climatological data, e.g. Global Mapping Function, GMF (Boehm et al., 2006a) or NWM data, e.g. Vienna Mapping Function, VMF (Boehm et al., 2006b). An advantage of the first approach is its independence of external data. Several mapping functions for tropospheric gradients have also been developed in the past, e.g. by Bar-Sever et al. (1998), by Chen and Herring (1997), or the tilting mapping function introduced by Meindl et al. (2004). The gradient mapping function (*mfg*) by Bar-Sever (BS) is given as

$$mfg = mfw * cot(ele) \quad (2)$$

and from the formula is apparent that it depends on the selected *mfw*. The Chen and Herring (CH) *mfg* reads as

$$mfg = 1 / (sin(ele) * tan(ele) + c) \quad (3)$$

where $c = 0.0032$. Since c is related to the scale height, it experiences spatiotemporal variations. Nevertheless, based on Balidakis et al. (2018) a variable c does not yield a statistically significant improvement in describing the atmospheric state over a constant c. Finally, the tilting mapping function is defined as a tilting of the *mfw* by using the so-called tropospheric zenith.

Figure 1 shows the fractional contribution of the tropospheric gradients to the slant total delay expressed in Eq. (1) as $(Gn * cos(a) + Ge * sin(a))$, i.e. the projection of the horizontal gradient vector in the direction of the individual satellites, as a function of a) the mapping factor represented by actual values of the *mfg* (left plot), and b) the observation elevation angle

Ann. Geophys. Discuss., https://doi.org/10.5194/angeo-2018-93
Manuscript under review for journal Ann. Geophys.
Discussion started: 10 September 2018

(right plot). The figure includes all GNSS observations in the benchmark campaign on one specific day (May 31, 2013). The x-range of gradient mapping factors clearly shows the difference in the three *mfg*. The tilting one gives the factors in between BS and CH *mfg* and, consequently, results in values in between them - the figure clearly shows the maximum values are inversely proportional to the maximum *mfg* factors. The black dots indicate values from a single epoch of the day (20:30 UTC).

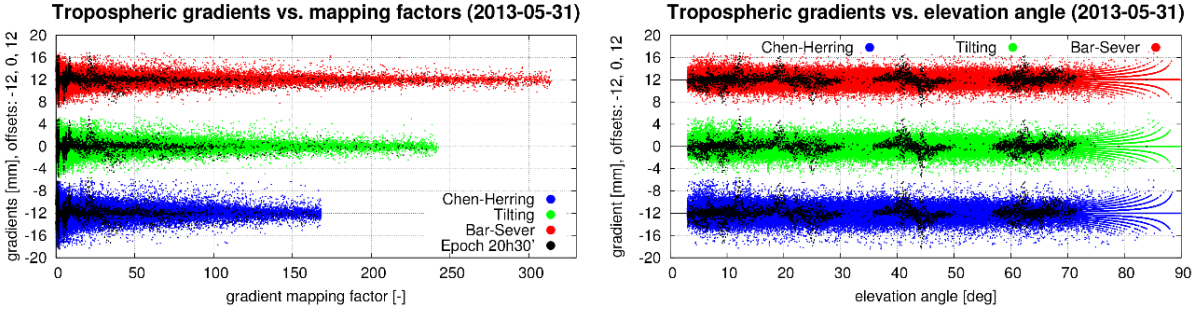

Figure 1. Dependence of tropospheric gradients expressed in satellites azimuth on gradient mapping factors (left) and elevation angles of actually contributing observations (right). Three *mfg* were studied on May 31, 2013: Chen and Herring *mfg* (blue), Bar-Sever *mfg* (red) and tilting *mfg* (green). Black dots show only values from 20:30 UTC.

We use the G-Nut/Tefnut software (Václavovic et al., 2014) for GNSS data processing of the benchmark campaign. This software utilizes the PPP method and is capable of multi-GNSS processing in real-time (RT), near-real time (NRT) and post-processing (PP) mode with a focus on all the tropospheric parameters estimation: ZTDs, gradients and slant delays (Douša et al., 2018b). Stochastic modelling of the troposphere allows an epoch-wise parameter estimation by extended Kalman filter in RT solutions (FLT) or its combination with a backward smoother which is used for NRT and PP solutions (FLT+SMT), see Václavovic and Douša (2015).

Table 1 describes all eight variants of solution for the benchmark campaign produced using the G-Nut/Tefnut which differ in (a) elevation cut-off angle (3° or 7°), (b) gradient mapping function (Chen and Herring = CH or Bar-Sever = BS), (c) constellations (GPS only = Gx or GPS+GLONASS = GR) and (d) processing mode (post-processing using the FLT+SMT processing or simulated real-time using the FLT processing only). All the variants except the three were based on the post-processing mode using the backward smoother and the ESA final orbit and clock products (http://navigation-office.esa.int/GNSS_based_products.html). Three additional solutions, abbreviated as RT1GxCH3, RT3GxCH3 and RTEGxCH3, were included to test the performance of the Kalman filter and RT orbit and clock corrections instead of a post-processed solution supported with final precise products. The solutions RT1GxCH3 and RT3GxCH3 simulate a real-time capability of estimates when using the IGS01 (RT1GxCH3) and IGS03 (RT3GxCH3) corrections from the IGS Real-Time Service (RTS, http://rts.igs.org). While IGS01 RTS product is a GPS only single-epoch solution produced using software developed by ESA/ESOC, the IGS03 product is a GPS+GLONASS solution based on a Kalman filter and the BKG's BNC software. The last solution, RTEGxCH3, applying the ESA final product is used to test a benefit of the backward smoothing on the one hand, and, an impact of the quality of RT corrections on the other hand. Unfortunately, the solution based on the

processing of GPS+GLONASS data in the simulated RT mode had to be rejected due to a highly variable quality of RT correction in 2013 affecting mainly the GLONASS contribution.

The GPT model was used for calculating a priori ZHDs and the GMF was used for mapping hydrostatic and wet delays to the zenith. Estimated tropospheric parameters are thus independent from any meteorological information. GNSS observations were processed using 30-hour data batches when starting six hours before the midnight of a given day in order to eliminate the PPP convergence. In all variants, the observation sampling of 300 s was used with ZTDs and tropospheric gradients estimated for every epoch. The station coordinates were estimated on a daily basis. The random walk of 6 mm/sqrt(hour) was applied for the ZTD and 1.5 mm/sqrt(hour) for the gradients. Absolute IGS model IGS08.ATX was used for the antenna phase centre offsets and variations. All variants used the elevation observation weighting of *1/sin2(ele)*.

Table 1. Processing parameters of individual variants from the G-Nut/Tefnut software. Mode FLT denotes to simulated real-time solution using Kalman filter only, FLT+SMT to post-processing solution using the Kalman filter and the backward smoother.

Solution name	Elevation cut-off	Constellation	Gradient mapping function	Products	Mode
GxCH3	3	GPS	Chen and Herring	ESA final	FLT+SMT
GRCH3	3	GPS+GLONASS	Chen and Herring	ESA final	FLT+SMT
GRBS3	3	GPS+GLONASS	Bar-Sever	ESA final	FLT+SMT
GxCH7	7	GPS	Chen and Herring	ESA final	FLT+SMT
GRCH7	7	GPS+GLONASS	Chen and Herring	ESA final	FLT+SMT
RT1GxCH3	3	GPS	Chen and Herring	IGS01 RT	FLT
RT3GxCH3	3	GPS	Chen and Herring	IGS03 RT	FLT
RTEGxCH3	3	GPS	Chen and Herring	ESA final	FLT

2.3 Estimation of tropospheric gradients from NWM

Tropospheric gradients and zenith delays were derived from the output of two different numerical weather models; the ERA5 (https://www.ecmwf.int/en/forecasts/datasets/archive-datasets/reanalysis-datasets/era5) and a simulation utilizing the Weather Research and Forecasting (WRF) model (Skamarock et al., 2008). The ERA5 is a reanalysis produced at the European Centre for Medium-Range Weather Forecasts (ECMWF). The pressure, temperature and specific humidity fields are provided with a horizontal resolution of approximately 31 km (T639 spectral triangular truncation) on 137 vertical model levels (up to 0.01 hPa). Although the ERA5 output is available every hour, we derived tropospheric parameters from it in 3-hour interval to avoid an extensive data handling. The WRF simulations are performed at GFZ Potsdam. The initial and boundary conditions for the limited area 24-hour free forecasts (starting every day at 0 UTC) stem from the analysis of the Global Forecast System (GFS) of the National Centers for Environmental Prediction (NCEP). The pressure, temperature and specific humidity fields are available every hour with a horizontal resolution of 10 km on 49 vertical model levels (up to 50 hPa).

The ray-trace algorithm by Zus et al. (2012) is used to compute STDs. The tropospheric gradients are derived from STDs as follows. At first, 120 STDs are computed at elevation angles 3°, 5°, 7°, 10°, 15°, 20°, 30°, 50°, 70°, 90° and all azimuths

between 0° and 360° with an interval of 30°). Second, we compute azimuth-independent STDs under the assumption of a spherically layered troposphere. Third, the differences between the azimuth-dependent STDs and the azimuth-independent STDs are computed. Finally, the gradient components are determined by a least-square fitting. For details the reader is referred to the Appendix in Zus et al. (2015).

Using ERA5 long-term global data, we experimented with different observation elevation weighting schemes (equal versus standard elevation angle dependent weighting) and two *mfg*s (BS and CH). While using different observation elevation weighting schemes led to negligible differences in the tropospheric gradients, we found a significant systematic difference in the north gradient component between tropospheric gradients derived with BS and CH *mfg* (see Appendix A). Since NWM derived tropospheric gradients presented in this study were computed using CH *mfg*, in principal their comparison with GNSS gradients estimated with BS *mfg* should be treated cautiously.

3 Impact of applied processing settings on GNSS tropospheric gradients estimation

ZTDs and tropospheric gradients from all eight variants were compared to each other and to the tropospheric parameters from ERA5 and WRF to evaluate the impact of various settings in GNSS data processing. Although about 430 GNSS stations are available in the benchmark data set, results given in this section are based on a subset of 243 stations. Firstly, 84 stations without the capability of receiving GLONASS signals were excluded. Secondly, stations which did not have at least 5 % of all the observations in the range of elevation angles between 3° and 7° were excluded as well. This rule was applied to allow a systematic evaluation of elevation cut-off angle impact on tropospheric parameters. The majority of the stations (103) had to be excluded because of inability to provide a sufficient number of observations at very low elevation angles.

Tropospheric parameters from the G-Nut/Tefnut software were provided every 5 minutes while the output from the WRF model was available every hour and the output from the ERA5 model was computed every three hours. Therefore, comparisons between GNSS solutions are based on a 5-minute interval while comparisons between GNSS and NWM solutions are based on a 3-hour interval.

3.1 Comparison of individual GNSS variants with each other

Results for individual GNSS variants comparison based on 3.6 million of pairs of values over 55 days and 243 GNSS stations are presented in Table 2. We notice a good agreement among all the post-processing (PP) variants from the statistics. The standard deviation (SDEV) indicates the smallest impact due to the change of *mfg* for both ZTD estimates (0.2 mm) and tropospheric gradients (~0.14 mm). The impact increases then slightly when comparing results of a single-/dual-constellation (1.2 mm for ZTD, ~0.18 mm for gradients). In dual-constellation, GLONASS observations were down-weighted by a factor of 1.5. The gradients estimated with improved geometry and using more observations are expected to provide more accurate and reliable estimates which is notable in the comparisons of single-/dual-constellation at different elevation cut-off angles.

Ann. Geophys. Discuss., https://doi.org/10.5194/angeo-2018-93
Manuscript under review for journal Ann. Geophys.
Discussion started: 10 September 2018

Generally, the largest impact is observed due to the elevation cut-off angle, i.e. 2.2 mm and ~0.21 mm for ZTD and tropospheric gradients, respectively.

There were no significant negative biases observed, but small biases of -0.05 mm and 0.03 mm for north and east gradient component, respectively, when comparing solutions using CH and BS mapping functions. These small systematic effects are attributed to the smaller tropospheric gradients computed with BS *mfg* compared to CH *mfg* (see Section 4). The larger effect can be found in the north-south direction reflecting the mean gradient (see Table 4) pointing towards the equator.

A penalty of RT processing versus PP ones is visible on standard deviation values for ZTD and tropospheric gradients increased by a factor of 3 and on significant biases. The two RT solutions can be still considered of good quality if we take into consideration results found in Ahmed et al. (2016) or Kačmařík (2018). Since no significant biases for both ZTD and tropospheric gradients were present in the RTEGxCH3 variant, when using the Kalman filter too, the quality of RT tropospheric parameters is mainly a consequence of a lower quality of IGS01 and IGS03 RT products.

Table 2. Comparison of individual variants of GNSS data processing run in post-processing mode (top) and in simulated real-time mode (bottom), units: mm.

Compared PP solutions	ZTD		N-S gradient		E-W gradient	
	BIAS	SDEV	BIAS	SDEV	BIAS	SDEV
GRCH3 – GRBS3	0.0	0.2	-0.05	0.15	0.03	0.13
GRCH3 – GxCH3	0.1	1.1	0.00	0.17	-0.02	0.16
GRCH7 – GxCH7	0.1	1.2	-0.01	0.20	-0.02	0.18
GRCH3 – GRCH7	0.1	2.1	0.01	0.20	0.00	0.18
GxCH3 – GxCH7	0.2	2.2	0.01	0.23	-0.01	0.21
Compared RT solutions	**ZTD**		**N-S gradient**		**E-W gradient**	
	BIAS	SDEV	BIAS	SDEV	BIAS	SDEV
GxCH3 – RT1GxCH3	-3.5	5.9	0.10	0.55	-0.18	0.57
GxCH3 – RT3GxCH3	-2.7	6.4	0.05	0.76	-0.08	0.80
GxCH3 – RTEGxCH3	-0.1	4.4	0.00	0.39	0.02	0.44
RT1GxCH3 – RT3GxCH3	0.8	5.0	-0.05	0.75	0.11	0.75

3.2 Comparison of individual GNSS variants with NWM

The statistics for the GNSS and NWM comparisons are summarized in Table 3. A bias of about 1 (4) mm is visible for ZTDs between GNSS and ERA5 with standard deviations around 9 (11) mm for individual PP (RT) GNSS solutions. The standard deviations are about 2 mm larger when GNSS and WRF are compared. This is probably due to the fact that the solution from WRF is based on a 24-hour free forecast (errors are supposed to grow with increasing forecast length) whereas the solution from ERA5 is based on a reanalysis. We attribute a negative bias of -3 mm in ZTD between GNSS and WRF to the global NCEP GFS analysis which is used for the initial and boundary conditions for the WRF solution. A negative bias of -5 mm in ZTD between two GNSS reference solutions and a solution based on the NCEP GFS was already reported in the past (Douša et al., 2016).

Ann. Geophys. Discuss., https://doi.org/10.5194/angeo-2018-93
Manuscript under review for journal Ann. Geophys.
Discussion started: 10 September 2018

Table 3. Comparison of individual variants of GNSS data processing run in post-processing mode (top) and in simulated real-time mode (bottom) with NWM solutions, units: mm.

Compared PP solutions	ZTD		N-S gradient		E-W gradient	
	BIAS	SDEV	BIAS	SDEV	BIAS	SDEV
GRCH3 – ERA5	1.0	8.8	-0.02	0.48	-0.01	0.48
GRBS3 – ERA5	1.0	8.9	0.03	0.42	-0.03	0.43
GxCH3 – ERA5	1.0	9.1	-0.01	0.49	0.01	0.48
GxCH7 – ERA5	0.8	10.2	-0.02	0.56	0.01	0.53
GRCH7 – ERA5	0.9	9.8	-0.03	0.54	-0.01	0.52
GRCH3 – WRF	-2.8	11.2	-0.04	0.54	-0.00	0.56
GRBS3 – WRF	-2.8	11.2	0.01	0.49	-0.02	0.52
GxCH3 – WRF	-2.8	11.4	-0.04	0.55	0.02	0.56
GxCH7 – WRF	-3.0	12.2	-0.04	0.61	0.03	0.61
GRCH7 – WRF	-2.9	11.9	-0.05	0.59	0.01	0.60
Compared RT solutions	**ZTD**		**N-S gradient**		**E-W gradient**	
	BIAS	SDEV	BIAS	SDEV	BIAS	SDEV
RT1GxCH3 – ERA5	4.5	10.3	-0.12	0.58	0.20	0.58
RT3GxCH3 – ERA5	3.6	10.7	-0.06	0.83	0.08	0.90
RTEGxCH3 – ERA5	1.0	9.6	-0.01	0.47	-0.01	0.46
RT1GxCH3 – WRF	0.7	12.6	-0.14	0.63	0.21	0.65
RT3GxCH3 – WRF	-0.2	12.8	-0.08	0.87	0.09	0.95
RTEGxCH3 – WRF	-2.8	11.9	-0.04	0.53	0.01	0.55
ERA5 - WRF	-3.8	11.0	-0.02	0.40	0.01	0.45

With regards to the tropospheric gradients, the biases between GNSS and NWM stayed within a range from -0.05 to 0.03 mm. The exception was the GNSS RT solution RT1GxCH3 with a bias of -0.1 mm for the north component and 0.2 mm for the east component. The standard deviations between GNSS and NWM were approximately doubled or tripled when compared to standard deviations between individual variants of GNSS solutions. They were also found to be higher for the WRF than for ERA5. Again, this can be probably explained by the fact that the solution from WRF is based on a 24-hour free forecast whereas ERA5 is based on a reanalysis.

Obviously, NWMs cannot be regarded as a ground truth. However, a similar pattern is present in results for both of them: standard deviations are smaller for GNSS solutions using a lower cut-off elevation angle (3° instead of 7°) and when using more observations (GPS+GLONASS). For example, the SDEV for north gradient component between GNSS and ERA5 is 0.56 mm for the GxCH7 variant while 0.48 mm for the GRCH3 variant. This represents a decrease of 14 %. From two GNSS variants differing only in the *mfg*, the solution applying the BS mapping function is closer to the NWMs in terms of standard deviation. This can be partly understood as the magnitudes (modulus of the gradient vector $\sqrt{Gn^2 + Ge^2}$) of GNSS tropospheric gradients using the BS *mfg* are smaller compared to the ones from the CH *mfg* (see next Section) and the magnitudes of NWM tropospheric gradients are in general smaller and more smoothed compared to the GNSS tropospheric gradients.

Ann. Geophys. Discuss., https://doi.org/10.5194/angeo-2018-93
Manuscript under review for journal Ann. Geophys.
Discussion started: 10 September 2018

Maps showing tropospheric gradients were generated for all the variants of GNSS solutions and both NWM solutions and visually evaluated for the whole benchmark period. For better visualization we included all the GNSS stations of the benchmark campaign, i.e. not just the subset of 243 stations used for the presented statistics. Generally, GNSS provided homogenous fields of tropospheric gradients without a noisy behaviour at the level of individual stations and a very good agreement in gradient directions and usually also in gradient magnitudes was found between GNSS and NWM gradient maps. In Figure 2, two examples are shown for different events when a weather front was passing over the studied area. Tropospheric gradients derived from NWM provided more smoothed gradient fields, but somehow limited to render local structures mainly due to the spatial resolution of both NWMs. As the ERA5 model has coarser spatial resolution than the WRF model, such behaviour was a little bit more apparent in its outputs. On the other hand, when compared to results of the 1° × 1° resolution global models ERA-Interim and NCEP GFS (Douša et al., 2016), the presented NWMs tropospheric gradients have larger magnitudes. A detailed evaluation of tropospheric gradient maps with meteorological observations will be a subject of an upcoming study.

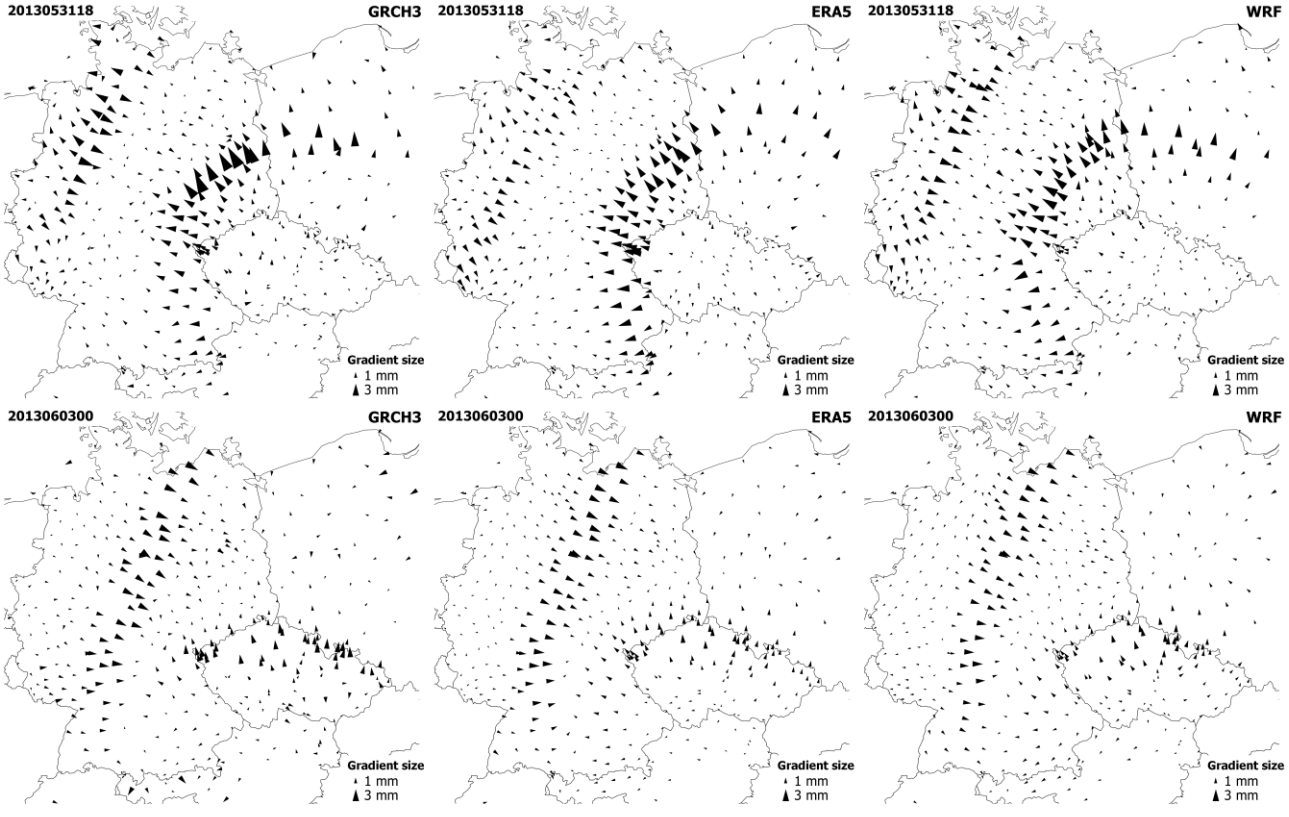

Figure 2. Tropospheric gradient maps from GNSS GRCH3 solution (left), NWM ERA5 solution (middle) and NWM WRF solution (right) on 31 May 2013, 18:00 UTC (top) and on 03 June 2013 00:00, UTC (bottom).

Comparing GNSS to NWM products in Table 3 indicated that the RTEGxCH3 solution driven by the Kalman filter and the ESA final product shows a comparable performance to the GxCH3 solution driven by the Kalman filter and the backward

Ann. Geophys. Discuss., https://doi.org/10.5194/angeo-2018-93
Manuscript under review for journal Ann. Geophys.
Discussion started: 10 September 2018

smoother. An increase of bias and standard deviation values for other solutions based on RT mode indicates that the quality of the RT tropospheric product is dominated by an actual quality of RT orbit and clock corrections. In this regard, we examined systematically all tropospheric gradient maps and found that gradients from the RTEGxCH3 solution are always in a very good agreement with PP solutions. Although there were imperfections in matching RT1GxCH3 gradients and PP solutions, the performance can be still considered as generally good and stable. This was however not the case of the RT3GxCH3 solution where we observed a varying quality of estimated tropospheric gradients. For the majority of epochs, in particular during the periods with strong gradients, the tropospheric gradients could be evaluated as acceptable. However, situations when gradients from all the stations point to the same direction occurred from time to time, obviously without a physical relation to the actual weather situation. An example of this behaviour is presented in Figure 3 where tropospheric gradients from the RT3GxCH3 solution behave normally on 31 May 2013, 18:00 UTC, and became unrealistic on 6 May 2013, 18:00 UTC where all the stations point to the south-west direction and reveal high gradient magnitudes. These issues occurred occasionally and for a limited period of time and in the RT3GxCH3 solution only. It happened most probably due to many interruptions (mainly in GLONASS RT corrections) which affected the quality of RT products and caused frequent PPP re-initialization.

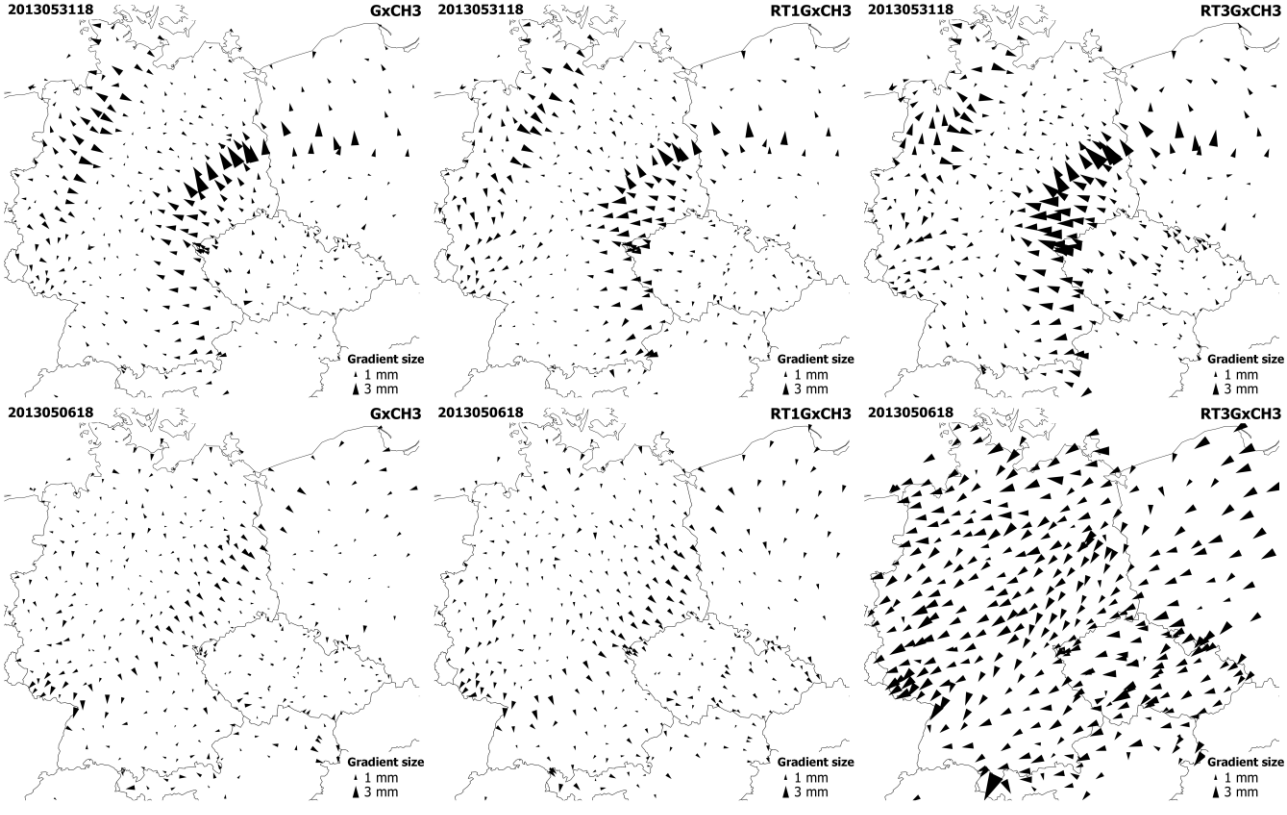

Figure 3. Tropospheric gradient maps from GNSS GxCH3 solution (left), GNSS RT1GxCH3 solution (middle) and GNSS RT3GxCH3 solution (right) on 31 May 2013, 18:00 UTC (top) and on 06 May 2013, 18:00 UTC (bottom).

Ann. Geophys. Discuss., https://doi.org/10.5194/angeo-2018-93
Manuscript under review for journal Ann. Geophys.
Discussion started: 10 September 2018

3.3 Additional assessment of processing settings on GNSS tropospheric gradients

Mean gradient magnitudes and azimuth angles (direction of gradient) over the whole benchmark period were computed for 243 GNSS stations and are presented in Table 4. Mean magnitudes of tropospheric gradients from all PP GNSS variants oscillated around 0.85 mm and 0.67 mm when using the CH *mfg* and the BS *mfg*, respectively. Gradients computed using the latter show about 17 % smaller gradients compared to the former if all the processing aspects remained identical. Both RT solutions also resulted with higher gradient magnitudes, namely +14 % for RT1GxCH3 and +47 % for RT3GxCH3 when compared to the corresponding GxCH3 PP variant. A mean gradient magnitude of about 0.7 mm was found for both NWM solutions, i.e. of about 0.1 mm smaller than for the GRCH3 solution. This can be mainly explained by the limited horizontal resolution of the NWMs.

Table 4 shows that mean tropospheric gradients point towards the equator, see also Meindl et al. (2004). Such a mean gradient direction does not depend on the gradient mapping function. By adding GLONASS observations the mean gradient direction was changed by +2°, however, actual effects were found to be highly station-dependent with a typical range of ±5° for individual stations. The direction of mean gradient in both NWM solutions was in a very good agreement with that in all GNSS solutions using GPS+GLONASS constellation.

Directions of mean gradient over individual stations were mostly within ±15° when compared to the total mean gradient estimated for the stations and the solution variant. On the other hand, the performance was not identical for the individual solutions. A change of cut-off elevation angle from 7° to 3° led to a significantly increased number of stations with the mean gradient direction within ±15° of the total mean direction and to a decreased number of stations with a mean gradient direction differing for more than 30° (regarded as outlier stations in Table 4). Two GNSS stations were marked as outliers by all processed variants with their mean gradient direction differing by more than 50° from the total variant mean. Both of them are located in a developed area in south-west Germany and are using the same receiver and antenna type from Leica, which is however used by many other stations in the same region where no issues with gradient mean angle were identified. Still, the reason of their different behaving can be of instrumental or environmental origin.

In Table 5, mean formal errors of ZTDs and both horizontal gradient components from GNSS data processing are examined for all the processed variants. Formal error of the parameter can be generally regarded as an estimation uncertainty. Typically, high formal errors for tropospheric parameters occur at situations when they were estimated under not favourable conditions, it means i.e. low number of observations and/or their poor geometry and/or their poor quality. Both for ZTDs and horizontal gradients a decrease of a mean formal error was occurring when more observations were used in the processing. This behaviour is logical and expectable since a higher number of observations is being used to estimate the same number of unknown parameters. On the other hand, when the solution GRCH7 using GPS+GLONASS observations and an elevation cut-off of 7 degrees was compared to the GRCH3 solution using the same constellation but a cut-off of 3 degrees, a decrease of formal error in horizontal gradients was approximately 16.5 % but the increase in number of observations between these two solutions was only 8 %. Since the decrease of formal error for ZTD in the same case was only 11 %, observations from very low elevation

angles affect here more the horizontal gradients estimation than ZTDs. Using the BS *mfg* gives generally smaller formal errors for tropospheric gradient estimates, but these do not differ significantly for any other estimated parameters when compared to any other *mfg*. It suggests to reflect only the impact of differences in mapping factors on calculating formal errors.

Table 4. Mean magnitudes and azimuth angles of tropospheric gradients from all individual GNSS variants of processing and NWMs ERA5 and WRF.

Solution	Mean magnitude (mm)	Mean azimuth (°)	Percentage of stations with mean azimuth = total_mean ± 15°	Percentage of stations with mean azimuth = total_mean ± 30°	Number of outlier stations
GRCH3	0.81	170.3	88.9	99.2	2
GRBS3	0.67	170.4	91.8	98.8	3
GxCH3	0.83	168.4	88.1	97.5	6
GxCH7	0.86	168.2	74.1	95.1	12
GRCH7	0.84	170.5	79.8	97.1	7
RT1GxCH3	0.95	152.4	92.6	97.9	5
RT3GxCH3	1.22	162.7	96.3	98.8	3
RTEGxCH3	0.75	168.7	86.0	97.5	6
ERA5	0.69	171.8	97.1	100.0	0
WRF	0.73	171.0	100.0	100.0	0

Table 5. Mean formal errors and their standard deviation for tropospheric parameters from individual GNSS processing variants.

GNSS solution	ZTD formal error		N gradient formal error		E gradient formal error	
	Mean (mm)	SDEV (mm)	Mean (mm)	SDEV (mm)	Mean (mm)	SDEV (mm)
GRCH3	3.81	0.37	0.81	0.10	0.81	0.09
GRBS3	3.82	0.37	0.74	0.09	0.75	0.09
GxCH3	4.28	0.46	0.93	0.13	0.90	0.13
GxCH7	4.84	0.44	1.14	0.14	1.05	0.14
GRCH7	4.28	0.36	0.99	0.10	0.95	0.11
RT1GxCH3	6.71	1.72	0.91	0.08	0.92	0.09
RT3GxCH3	7.09	1.76	1.50	0.22	1.53	0.22
RTEGxCH3	6.60	0.67	0.91	0.08	0.92	0.08

4 Systematic effects of GNSS tropospheric gradients estimation

In this section, we focus on systematic differences induced by utilizing different *mfg* and observation elevation-dependent weighting (OEW). For two solutions defined in Section 2.2 and utilizing CH *mfg* (GRCH3) and BS *mfg* (GRBS3), we additionally generated four variants using various OEW schemes: 1) EQUAL, equal weighting, 2) SINEL1, $1/\sin(ele)$, 3) SINEL2, $1/\sin^2(ele)$, and 4) SINEL4, $1/\sin^4(ele)$. The contribution of low-elevation observations to all estimated parameters decreases with increasing power y in $1/\sin^y(ele)$. As a consequence, the magnitude of tropospheric gradients is reduced due to the strong dependence on such observations. The impact of the *mfg* on the estimated tropospheric gradients is then reduced

Ann. Geophys. Discuss., https://doi.org/10.5194/angeo-2018-93
Manuscript under review for journal Ann. Geophys.
Discussion started: 10 September 2018

too. These variants were provided for May 31, 2013 which is an interesting day due to an occlusion front present over Germany, and captured by strong tropospheric gradients both from GNSS and NWM.

Figure 4 displays maps of tropospheric gradients on May 31, 2013 (18:00 UTC) from both GRBS3 and GRCH3 solutions when applying two selected schemes of OEW (EQUAL and SINEL2). This particular epoch shows a significant difference in magnitudes of estimated gradients. Figure 5 then shows a cumulative systematic difference (over all epochs in May 31, 2013) in north and east gradient components between two *mfg* and OEWs. In this case, the systematic difference clearly depends on both magnitudes and direction of gradients. A positive difference can be seen for the north gradient component when the actual gradient points to north and east component when the actual gradient points to east. Negative differences occurred when gradients were pointing to the opposite directions. A maximum systematic difference was observed for the EQUAL OEW, while it has been reduced for the SINEL1 weighting (not shown) and further for the SINEL2 weighting. A systematic difference has been almost eliminated when using the SINEL4 weighting (not shown). Generally, all the OEW schemes demonstrate a strong impact of low-elevation observations reflecting an actual local tropospheric asymmetry in the water vapour distribution.

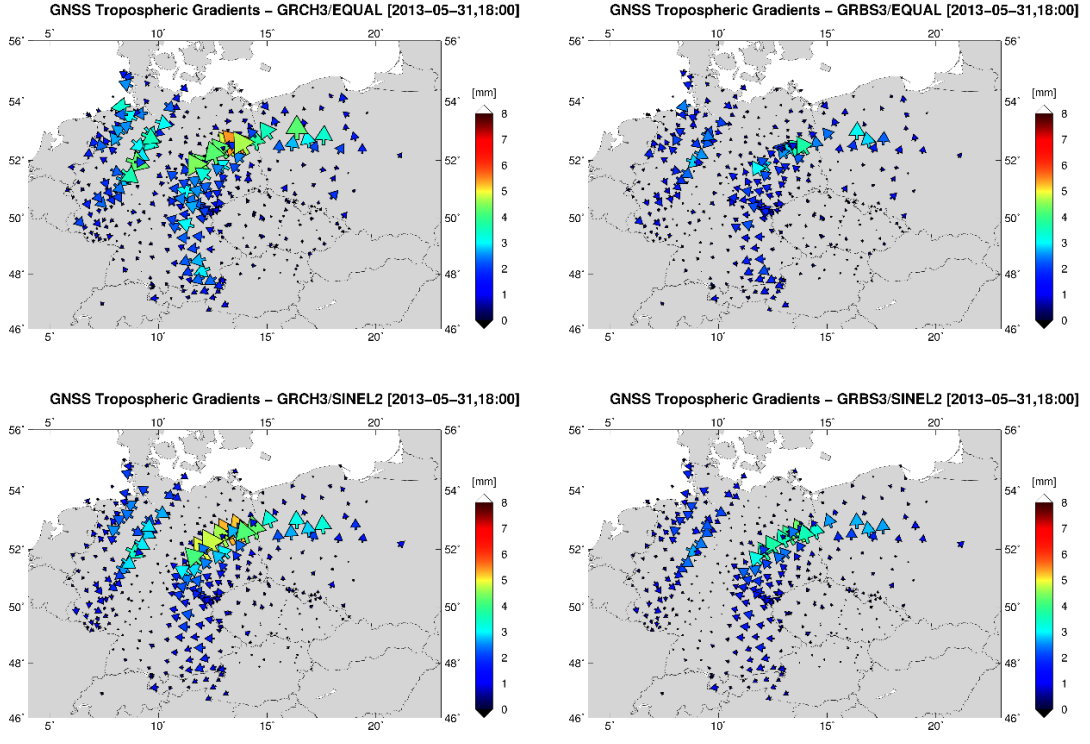

Figure 4. Tropospheric gradient maps on May 31, 2013 (18:00 UTC) from GNSS solutions using: Chen and Herring *mfg* (left), Bar-Sever *mfg* (right) and EQUAL (top) and SINEL2 (bottom) observation weighting schemes.

Ann. Geophys. Discuss., https://doi.org/10.5194/angeo-2018-93
Manuscript under review for journal Ann. Geophys.
Discussion started: 10 September 2018

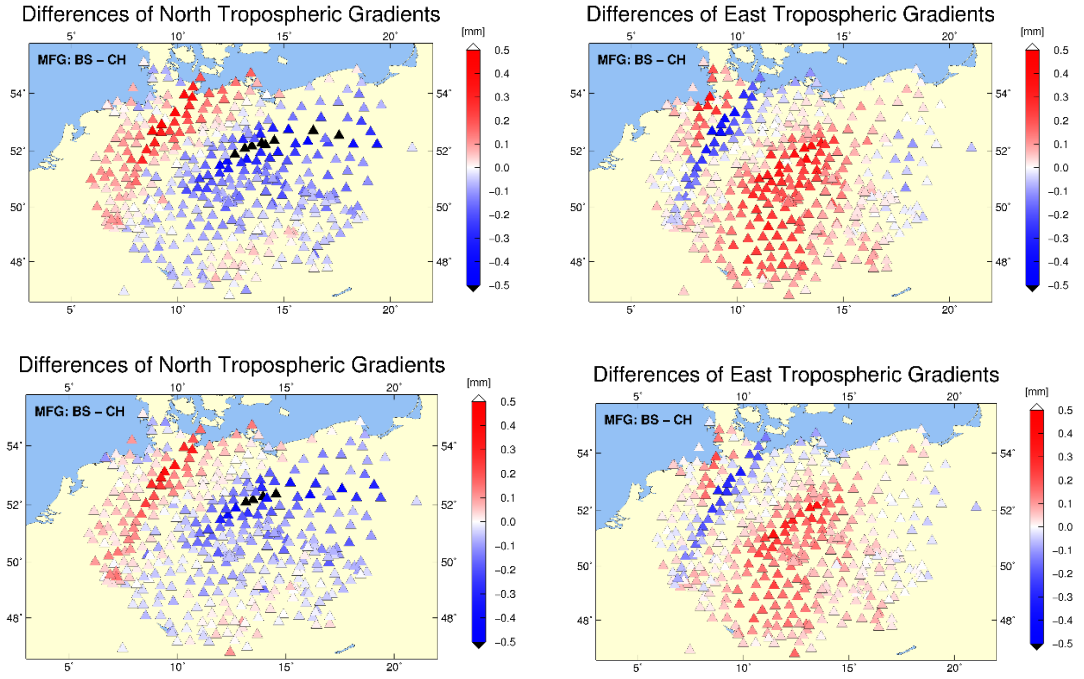

Figure 5. Mean differences of tropospheric gradient north component (left) and east component (right) due to different *mfg*: Chen and Herring (CH), Bar-Sever (BS) when using the EQUAL (top) and SINEL2 (bottom) observation weighting schemes. The differences are cumulated over full day May 31, 2013.

Figure 6 finally displays carrier-phase post-fit residuals with respect to the elevation for selected solutions. The SINEL2 OEW scheme in the left panel shows more homogenous distribution of carrier-phase post-fit residuals above the elevation angle of 30° when compared to the EQUAL scheme (right panel). While the *mfg* selection impacts SINEL2 residuals on a few millimetre-level below 15°, the EQUAL residuals could be affected at any elevation angles even up to the zenith direction. Generally, the SINEL2 results in a more realistic view considering the errors in GNSS observations which are expected to increase with a decrease of elevation angle, besides atmospheric ones we mean e.g. multipath effects, uncertainty of phase centre variations, lower signal-to-noise ratio, obstructions or cycle slips.

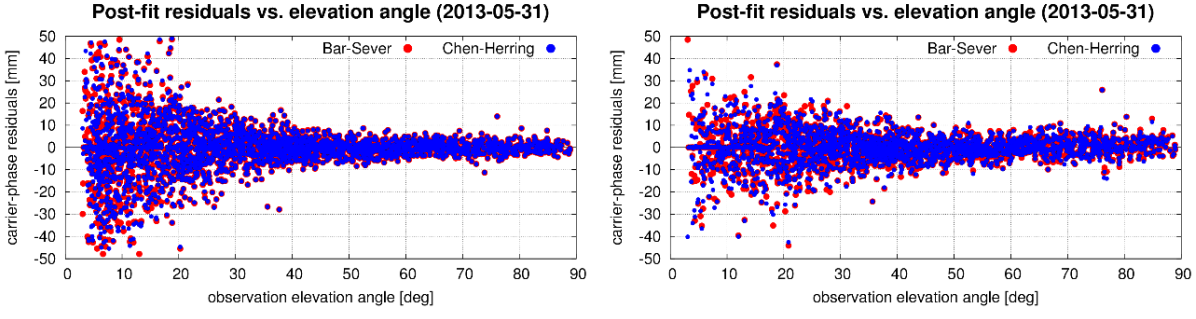

Figure 6. Post-fit phase residuals distribution when using different gradient mapping functions, Bar-Sever (red) and Chen and Herring (blue), and observation weighting: SINEL2 (left) and EQUAL (right).

Ann. Geophys. Discuss., https://doi.org/10.5194/angeo-2018-93
Manuscript under review for journal Ann. Geophys.
Discussion started: 10 September 2018

5. Conclusions

We presented an impact assessment of selected GNSS processing settings on estimated tropospheric gradients together with an evaluation of systematic differences resulting from gradient mapping function and observation elevation weighting. Primarily, we exploited the GNSS4SWEC benchmark campaign of 430 GNSS reference stations and two months of data in 2013 during severe weather event occurrence. ZTD values and tropospheric gradients were estimated in eight variants of GNSS data processing and derived from two NWMs (a global reanalysis and a limited area short range forecast).

Statistical comparisons and a systematic visual inspection of tropospheric gradient maps demonstrated that all post-processing solutions can be regarded as robust and their gradient estimates are clearly related to real weather conditions. Solutions provided tropospheric parameters in high temporal resolution (5 minutes) which are fully independent of meteorological input data, and besides the ZTD, tropospheric gradients thus provide additional interesting information in support of NWM forecasts.

A positive impact of a lower cut-off elevation angle (from 7° to 3°) suggested more robust tropospheric gradient estimates. Better agreements were observed between single- and dual- constellation products, when comparing to NWM gradients (a decrease of standard deviation of 10 %) and when analysing station-wise mean gradient directions. This finding is in a full agreement with Meindl et al. (2004) where a positive impact of using cut-off elevation angle of 3° instead of 10° was also reported.

A small impact only was observed by adding GLONASS observations (a decrease of standard deviation of 2 % in comparison with NWM gradients). This indicates that the post-processing tropospheric gradients can be well estimated already with using GPS satellites when the quality of such gradients obviously benefit from very low elevation angle observations.

Using a simulated real-time processing mode, the agreement of GNSS versus NWM tropospheric gradients revealed an increase in standard deviation of about 17 % (75 %) for IGS01 (IGS03) RT products when compared to the corresponding GNSS post-processing gradients. We also show that the quality of real-time tropospheric parameters is dominated by the quality of real-time orbit and clock corrections, and to a much lesser extent by the processing mode, i.e. Kalman filter without backward smoothing. Tropospheric gradients from the RT solution using the IGS03 RT product showed occasionally a large misbehaving of tropospheric gradients at all GNSS stations obviously not related to weather conditions. This was caused by PPP re-initializations due to interruptions and worse quality of the IGS03 RT product, while normal results were achieved by using the IGS01 RT product.

We studied systematic differences in estimated tropospheric gradients. Unlike for ZTDs, mean systematic differences up to 0.5 mm over a day (and even larger for a single epoch) can affect the magnitude of estimated tropospheric gradients due to utilizing different gradient mapping functions or elevation-dependent weightings. This difference was observed between Bar-Sever and Chen and Herring *mfg* while the tilting *mfg* behaves in between these two. These differences are observed in magnitudes of the gradients, but not in directions. However, the gradient direction results in different signs and scales of the two estimated gradient components. A long-term mean gradient pointing in a global scope to the equator causes systematic differences up to 0.3 mm in the north gradient component between Bar-Sever and Chen and Herring *mfg* (see Appendix A).

Ann. Geophys. Discuss., https://doi.org/10.5194/angeo-2018-93
Manuscript under review for journal Ann. Geophys.
Discussion started: 10 September 2018

Finally, it is hard to assess which *mfg* is more suitable for the troposphere modelling in GNSS analyses as we are missing accurate products that could be accepted as ground truth. Smaller gradient formal errors from Bar-Sever *mfg* are mainly attributed to larger mapping functions, while the better agreement with NWMs is due to the fact that the limited horizontal resolution of the NWMs yields smaller gradients in general. In any case it is necessary to agree on the *mfg* at least when tropospheric gradients derived from various sources (GNSS, WVR or NWM) are to be compared or combined.

Appendix A

In Figure 7 the systematic difference in the derived tropospheric gradients based on ERA5 data (average over 10 years) is shown for any point on Earth's surface between tropospheric gradients estimated utilizing the BS *mfg* and tropospheric gradients estimated utilizing the CH *mfg*. Whereas there is no considerable bias in the east gradient component, the mean bias reaches up to 0.3 mm in the north gradient component (positive in the northern and negative in the southern hemisphere). We note that the mean tropospheric gradients point to the equator (see Section 3.3), i.e., the north gradient component is negative in the northern hemisphere and positive in the southern hemisphere. This is due to the fact that the mean zenith delays increase towards the equator (see e.g. Meindl et al., 2004). The systematic difference between these two *mfg*s is due to the fact that for the same slant total delays the magnitude of gradients which are estimated utilizing a smaller *mfg* are larger than the magnitude of gradients which are estimated utilizing a larger *mfg*. The product of the *mfg* and the tropospheric gradients, i.e., the azimuth-dependent part of the tropospheric delay, remains approximately the same.

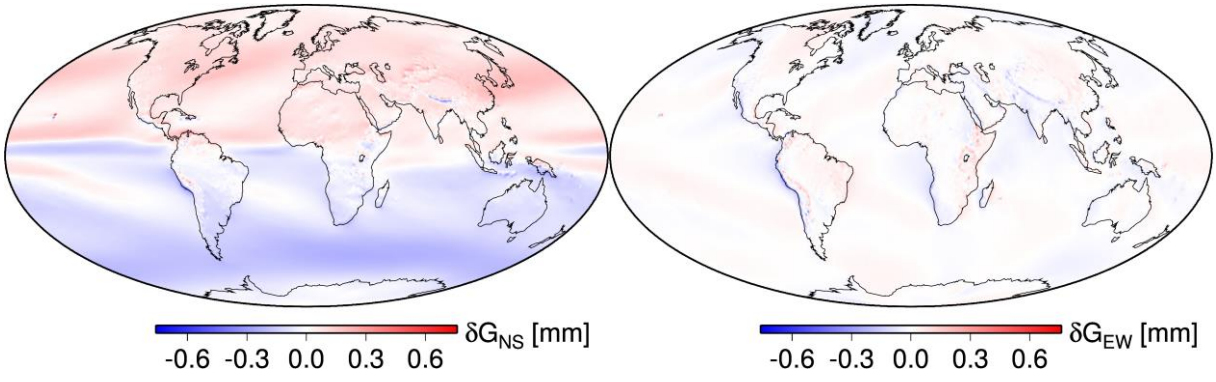

Figure 7. Systematic difference (average over 10 years) for any point on Earth's surface between tropospheric gradients estimated utilizing the gradient mapping function of Bar-Sever and tropospheric gradients estimated utilizing the gradient mapping function of Chen and Herring. The left panel shows the north gradient component, the right panel the east gradient component. The result is based on ERA5 data.

Acknowledgement

The authors thank all the institutions which provided GNSS observations for the COST ES1206 Benchmark campaign (Douša et al., 2016). F.Z. wants to thank Dr. Thomas Schwitalla (Institute of Physics and Meteorology, University Hohenheim) for

the introduction to the WRF system. The ECMWF is acknowledged for making publicly available ERA5 reanalysis fields that were generated using Copernicus Climate Change Service Information 2018 (https://www.ecmwf.int/en/forecasts/datasets/archive-datasets/reanalysis-datasets/era5). The GFS analysis fields are provided by the National Centers for Environmental Prediction (http://www.ftp.ncep.noaa.gov/data/nccf/com/gfs/prod). The study was realized during a mobility of M.K. at GFZ Potsdam funded by the EU ESIF project No. CZ.02.2.69/0.0/0.0/16_027/0008463. J.D. and P.V. acknowledge the Ministry of the Education, Youth and Science of the Czech Republic for financing the study with the project No LO1506.

References

Ahmed, F., Václavovic, P., Teferle, F.N., Douša, J., Bingley, R. and Laurichesse, D.: Comparative analysis of real-time precise point positioning zenith total delay estimates, GPS Solutions, 20, 187, doi:10.1007/s10291-014-0427-z, 2016.

Bar-Sever, Y.E., Kroger, P.M. and Borjesson, J.A.: Estimating horizontal gradients of tropospheric path delay with a single GPS receiver. Journal of Geophysical Research, 103, B3, 5019–5035, doi:10.1029/97JB03534, 1998.

Balidakis, K., Nilsson, T., Zus, F., Glaser, S., Heinkelmann, R., Deng, Z. and Schuh, H.: Estimating Integrated Water Vapor Trends From VLBI, GPS, and Numerical Weather Models: Sensitivity to Tropospheric Parameterization, Journal of Geophysical Research: Atmospheres, 123, 6356-6372, doi: 10.1029/2017JD028049, 2018.

Bender, M., Dick, G., Ge, M., Deng, Z., Wickert, J., Kahle, H.-G., Raabe, A. and Tetzlaff, G.: Development of a GNSS water vapour tomography system using algebraic reconstruction techniques, Advances in Space Research, 47, 10, p. 1704-1720, 2011.

Bender, M., Stephan, K., Schraff, C., Reich, H., Rhodin, A. and Potthast, R.: GPS Slant Delay Assimilation for Convective Scale NWP. Fifth International Symposium on Data Assimilation (ISDA), University of Reading, UK, July 18–22, 2016.

Boehm, J., Niell, A., Tregoning, P. and Schuh, H.: Global mapping function (GMF): A new empirical mapping function based on numerical weather model data, Geophysical Research Letters, 33, 943–951, doi:10.1029/2005GL025546, 2006a.

Boehm, J., Werl, B. and Schuh, H.: Troposphere mapping functions for GPS and very long baseline interferometry from European Centre for Medium-Range Weather Forecasts operational analysis data, Journal of Geophysical Research, 111, B02406, doi:10.1029/2005JB003629, 2006b.

Boehm, J., Heinkelmann, R. and Schuh, H.: Short note: A global model of pressure and temperature for geodetic applications, Journal of Geodesy, 81, 679–683, doi:10.1007/s00190-007-0135-3, 2007.

Brenot, H., Neméghaire, J., Delobbe, L., Clerbaux, N., Meutter, P., Deckmyn, A., Delcloo, A., Frappez, L. and Van Roozendael, M.: Preliminary signs of the initiation of deep convection by GNSS, Atmospheric Chemistry and Physics, 13, 5425–5449, doi:10.5194/acp-13-5425-2013, 2013.

Chen, G. and Herring, T. A.: Effects of atmospheric azimuthal asymmetry on the analysis of space geodetic data, Journal of Geophysical Research, 102, 20489–20502, doi:10.1029/97JB01739, 1997.

Douša, J., Dick, G., Kačmařík, M., Brožková, R., Zus, F., Brenot, H., Stoycheva, A., Möller, G. and Kaplon, J.: Benchmark campaign and case study episode in central Europe for development and assessment of advanced GNSS tropospheric models and products, Atmospheric Measurement Techniques, 9, 2989–3008, doi:10.5194/amt-9-2989-2016, 2016.

Douša, J., Václavovic, P. and Eliaš, M.: Tropospheric products of the second European GNSS reprocessing (1996-2014), Atmospheric Measurement Techniques, 10, 3589–3607, doi:10.5194/amt-10-3589-2017, 2017.

Douša, J., Eliaš, M., Václavovic, P., Eben, K. and Krč, P. A two-stage tropospheric correction combining data from GNSS and numerical weather model, GPS Solutions, 22, 77, doi:10.1007/s10291-018-0742-x, 2018a.

Douša, J., Václavovic, P., Zhao, L. and Kačmařík, M.: New Adaptable All-in-One Strategy for Estimating Advanced Tropospheric Parameters and Using Real-Time Orbits and Clocks, Remote Sensing, 10, 232, doi:10.3390/rs10020232, 2018b.

Flores, A., Ruffini, G. and Rius, A.: 4D tropospheric tomography using GPS slant wet delays, Ann. Geophys., 18, 223–234, doi:10.1007/s00585-000-0223-7, 2000.

Guerova, G., Bettems, J. M., Brockmann, E. and Matzler, C.: Assimilation of COST 716 Near-Real Time GPS data in the nonhydrostatic limited area model used at MeteoSwiss, Meteorol. Atmos. Phys., 91, 149–164, doi:10.1007/s00703-005-0110-6, 2006.

Iwabuchi, T., Miyazaki, S., Heki, K., Naito, I. and Hatanaka, Y.: An impact of estimating tropospheric delay gradients on tropospheric delay estimations in the summer using the Japanese nationwide GPS array, Journal of Geophysical Research, 108, D10, 4315, doi:10.1029/2002JD002214, 2003.

Järvinen, H., Eresmaa, R., Vedel, H., Salonen, K., Niemelä, S. and de Vries, J.: A variational data assimilation system for ground-based GPS slant delays, Q. J. R. Meteorol. Soc., 133, 969–980, doi:10.1002/qj.79, 2007.

Kačmařík, M.: Retrieving of GNSS Tropospheric Delays from RTKLIB in Real-Time and Post-processing Mode, In Lecture Notes in Geoinformation and Cartography, Proceedings of GIS Ostrava 2017, Ivan, I., Horák, J., Inspektor, T., Springer, Cham, doi:10.1007/978-3-319-61297-3_13, 2018.

Kawabata, T., Shoji, Y., Seko, H. and Saito, K.: A Numerical Study on a Mesoscale Convective System over a Subtropical Island with 4D-Var Assimilation of GPS Slant Total Delays, Journal of the Meteorological Society of Japan, 91, 705–721, doi:10.2151/jmsj.2013-510, 2013.

Li, X., Zus, F., Lu, C., Ning, T., Dick, G., Ge, M., Wickert, J. and Schuh, H.: Retrieving high-resolution tropospheric gradients from multiconstellation GNSS observations, Geophysical Research Letters, 42, 4173–4181, doi: 10.1002/2015GL063856, 2015.

Meindl, M., Schaer, S., Hugentobler, U. and Beutler, G.: Tropospheric Gradient Estimation at CODE: Results from Global Solutions, Journal of the Meteorological Society of Japan, 82, 1B, 331-338, doi:10.2151/jmsj.2004.331, 2004.

Morel, L., Pottiaux, E., Durand, F., Fund, F., Boniface, K., de Oliveira, P.S. and Van Baelen, J.: Validity and behaviour of tropospheric gradients estimated by GPS in Corsica, Advances in Space Research, 55, 135-149, doi:10.1016/j.asr.2014.10.004, 2015.

Rothacher, M. and Beutler, G.: The role of GPS in the study of global change, Physics and Chemistry of the Earth, 23, 9-10, doi:10.1016/S0079-1946(98)00143-8, 1998.

Saastamoinen, J.: Atmospheric Correction for the Troposphere and Stratosphere in Radio ranging of satellites, Geophy. Monog. Series, 15, 247–251, doi:10.1029/gm015p0247, 1972.

Shoji, J., Nakamura, H., Iwabuchi, T., Aonashi, K., Seko, H., Mishima, K., Itagaki, A., Ichikawa, R. and Ohtani, R.: Tsukuba GPS dense net campaign observation: Improvement in GPS analysis of slant path delay by stacking one-way postfit phase residuals, Journal of the Meteorological Society of Japan, 82, 301–314, doi:10.2151/jmsj.2004.301, 2004.

Shoji, Y., Kunii, M. and Saito, K.: Assimilation of Nationwide and Global GPS PWV Data for a Heavy Rain Event on 28 July 2008 in Hokuriku and Kinki, Japan. Scientific Online Letters on the Atmosphere, 5, 45–48, doi:10.2151/sola.2009-012, 2009.

Skamarock, W.C., Klemp, J.B., Dudhia, J., Gill, D.O., Barker, D.M., Duda, M.G., Huang, X.Y., Wang, W. and Powers, J.G.: A description of the advanced research WRF version 3. NCAR tech. note NCAR/TN-475+STR, doi:10.5065/D68S4MVH, 2008.

Václavovic, P., Douša, J. and Györi, G.: G-Nut software library - State of development and first results, Acta Geodynamica et Geomaterialia, 10, 4, 431-436, doi:10.13168/AGG.2013.0042, 2014.

Václavovic, P. and Douša, J.: Backward smoothing for precise GNSS applications, Advances in Space Research, 56, 8, 1627-1634, doi:10.1016/j.asr.2015.07.020, 2015.

Vedel, H. and Huang, X.: Impact of Ground Based GPS Data on Numerical Weather Prediction, Journal of the Meteorological Society of Japan, 82, 459–472, doi:10.2151/jmsj.2004.459, 2004.

Zhou, F., Li, X., Li, W., Chen, W., Dong, D., Wickert, J. and Schuh, H.: The Impact of Estimating High-Resolution Tropospheric Gradients on Multi-GNSS Precise Positioning, Sensors, 17, 756, doi:10.3390/s17040756, 2017.

Zumberge, J. F., Heflin, M. B., Jefferson, D. C., Watkins, M. M. and Webb, F. H.: Precise point positioning for the efficient and robust analysis of GPS data from large networks, Journal of Geophysical Research, 102, 5005–5017, doi:10.1029/96JB03860, 1997.

Zus, F., Bender, M., Deng, Z., Dick, G., Heise, S., Shang-Guan, M. and Wickert, J.: A methodology to compute GPS slant total delays in a numerical weather model, Radio Science, 47, RS2018, doi:10.1029/2011RS004853, 2012.

Zus, F., Dick, G., Heise, S. and Wickert, J.: A forward operator and its adjoint for GPS slant total delays, Radio Science, 50, 393–405, doi: 10.1002/2014RS005584, 2015.